RSC Advances

ROYAL SOCIETY OF CHEMISTRY

www.rsc.org/advances

Simultaneously remove nickel and phosphorus from spent electroless nickel plating wastewater via calcined Mg–Al–CO_3 hydroxides

Mingming Sun[a], Jixin, Su[a*], Siming Liu[a], Dongming, Wang[a], Wenbao Yan[a], Lin Zhang[a], Yuxin, Xiao[a], Xue Gao[a]

[a]School of Environmental Science and Engineering, Shandong University, Jinan 250100, China

*Phone: +86-531-88362008; fax: +86-531-88362008;

E-mail address: jxsu@ sdu. edu.cn

ABSTRACT

For electroless nickel plating wastewater, a novel approach for simultaneous removal of nickel and phosphorus on calcined Mg–Al–CO_3 hydroxides (CLDHs) was proposed. The dependence of adsorption efficiency on several parameters, including initial ions concentration, temperature, contact time and pH, has been investigated with batch experiments. Adsorption kinetics data of nickel and phosphorus could be well depicted by pseudo-second-order model. Adsorption isotherms studies showed that the uptake of nickel and phosphorus on CLDHs followed Langmuir and Freundlich models, respectively, and maximum removal of nickel or phosphorus was up to 22.87 or 761.5 mg/g. Thermodynamic analysis implied the adsorption process of nickel or phosphorus on CLDHs was spontaneous and endothermic. Further, the possible mechanisms were explored: in low concentration solutions, CLDHs occurred to reconstitution involving the isomorphous substituting sites of magnesium by nickel in sheets and concomitant utilization of phosphorus by the generated superficial sheets;

in high concentration solutions, CLDHs rebuilding hydrotalcites structures were influenced and formed mixed metal salts of phosphites, hydroxides, hypophosphites, which attributed to the presence of plentiful phosphorus and brought about the reduced uptake of nickel.

Keywords

Electroless nickel plating wastewater, Calcined hydroxides, Adsorption, Nickel and phosphorus, Simultaneous removal

1. Introduction

Due to the excellent physicochemical properties of coatings (e.g. homogeneity, high hardness, wearability and corrosion resistance, etc.), the electroless nickel (EN) plating technique has been widely applied in automotive, aerospace, plastic, machinery, packaging and electronic computer industries.[1, 2] Specifically, in the fastest-growing electronics industries, the EN plating technique enables metalizing plastic or glass parts surface to decorate or improve functionality, which is closely related to our daily necessities, for instance cell phone' shells. For the electroless nickel plating technique, the chemical reaction can be expressed as:

$$3NaH_2PO_2 + NiSO_4 \longrightarrow Ni + 2H_2 + 2P + 4NaH_2PO_3 + Na_2SO_4 \quad (1)$$

During the electroless Ni–P plating process, both concentrations of phosphites and organic compounds gradually accumulate to an unavailable level as the cycle continues.[3] Plenty of spent wastewater is produced with high quantities of nickel ions and phosphites, and small amount of hypophosphites and organic acids. Like other potentially toxic metals, nickel cannot be decomposed, and the toxicity is gradually

increased because of accumulation in living organisms and consequent biomagnification in the food chain, which may result in cancer.[4, 5] On the other hand, although phosphorus is a crucial element for organisms growth in ecosystems and environments, excess phosphate can cause aquatic eutrophication, especially in enclosed systems, leading to overgrowth of aquatic plants, depletion of dissolved oxygen, and even death of fish and other aquatic organisms.[6] Phosphate also can improve the contents of Biological Oxygen Demand (BOD) and Chemical Oxygen Demand (COD) in wastewater increasing disposal difficulty. Hence, it is of utmost importance for the removal of nickel and phosphorus from the spent EN plating wastewater by using an effective and robust technique.

Several approaches have been proposed to treat spent EN plating wastewater, such as alkaline precipitation, ion exchange, electrodialysis, adsorption, membrane filtration and solvent extraction.[7, 8] Among which, alkaline precipitation is the most common; however, the high buffer capacity from organic substances demands excessive amounts of chemicals to neutralize alkalinity. The precipitated sludge contains extremely hazardous waste of nickel hydroxides and thus must be further controlled. It is worth noting that the above methods are mainly focused on nickel removal, whereas less attention has been paid to the high concentration of phosphite. Herein, it is essential to develop a cost – effective and facile technique to simultaneously remove nickel and phosphorus from EN plating wastewater.

Layered double hydroxide (LDHs), a class of anionic clays with 2D-nanostructure, [9] can be expressed with a general formula of $[M_{1-x}^{2+} M_x^{3+} (OH)_2] (A^{n-})_{x/n} \cdot yH_2O$,

where M^{2+} is the divalent cation (Mg^{2+}, Ni, Cu^{2+}, etc.); M^{3+} is the trivalent cation (Al^{3+}, Fe^{3+}, Cr^{3+}, etc.); A^{n-} is the n-valent anion (inorganic, organic, complex and bioorganic) and x can have various values between 0.17 and 0.33.[10] Because of the special structures of LDHs, Zhou et al.[11] and Xu et al.[12] utilized the ions in electroplating wastewaters forming LDHs precipitates to purify themselves. Although certain positive results did have been achieved, the key focus was only to remove metal ions. Recently, Zhu et al. simultaneously recovered Ni, P and S from spent electroless nickel plating by forming graphene/NiAl hydroxides,[13] however, the process was complicated and required extra H_2O_2 inducing high cost. Previous studies have demonstrated that LDHs and calcined LDHs (CLDHs) can be used for removing anions and metallic cations. Moreover, CLDHs (M_{1-x}^{2+} M_x^{3+} $O_{1+x/2}$) possesses higher adsorption capacity than LDHs owing to the unique property known as "memory effect", which can spontaneously reconstruct the layered structure via rehydration, isomorphous substituting sites of metallic elements in sheets and incorporating of anions into interlayers from the aqueous solution.[14-16] Literature research indicated that massive work are confined to treat simulated wastewater containing anions via CLDHs, yet few study on CLDHs disposing metal-containing industrial wastewater. To the best of our knowledge, no study has been done on the co-adsorption of metallic cations (Ni^{2+}) and anions ($H_2PO_3^-$/$H_2PO_2^-$) in spent EN plating wastewater.[17]

In this study, a novel feasible approach using CLDHs as a low-cost adsorbent for the co-treatment of nickel and phosphorus in electroless nickel plating wastewater was presented. To explore the adsorption performance of CLDHs, the effects of several

parameters, such as ions initial concentration, temperature, contact time and pH were investigated. In the virtue of X-ray diffraction (XRD), Fourier transform infrared spectra (FTIR), Scanning Electron Microscopy (SEM), Electron dispersive X-ray analysis (EDX) and X-ray photoelectron spectroscopy (XPS) technologies, the possible adsorption mechanism was further elucidated.

2. Experimental

2.1. Materials

The chemicals, Mg $(NO_3)_2 \cdot 6H_2O$, Al $(NO_3)_3 \cdot 9H_2O$, NH_4HCO_3 and $NH_3 \cdot H_2O$ were of analytical purity and used as received. The industrial spent EN plating wastewater containing high quantities of nickel ions (Ni^{2+}) and phosphites ($H_2PO_3^-$), and small amount of hypophosphites ($H_2PO_2^-$) and organic acids (lactic acid and acetic acid, etc.), were used as stock solutions. The initial concentration of nickel (Ni) or phosphorus (P, phosphites and hypophosphites) was about 2.5 g/L and 200 g/L, respectively. Deionized water was used in all experiments.

2.2. Synthesis of the LDHs and CLDHs

$Mg_3Al–CO_3$ hydrotalcites (LDHs) were prepared by co-precipitation method with constant pH (10 ± 0.5).[18] One solution (400 mL) contained $Mg(NO_3) \cdot 6H_2O$ (0.12 mol) and $Al(NO_3)_3 \cdot 9H_2O$ (0.04 mol). A second solution (250 ml) contained 0.015 mol NH_4HCO_3 and 0.48 mol $NH_3 \cdot H_2O$. At room temperature, two solutions were simultaneously added drop wise to 400 mL of deionized water with continuously stirring. The resulting slurry was stirred to age for a specified period. The final precipitate was filtered, washed, and dried during 24 h at 80 °C to obtain LDHs. Calcined $Mg_3Al–CO_3$ hydrotalcites (CLDHs) were obtained by calcining LDHs in a

112 muffle furnace at 450 °C during 2 h and placed in desiccators for the following
113 experiments.

114 **2.3. Adsorption experiments**

115 Batch experiments were conducted with the industrial spent EN plating wastewater to
116 investigate sorption capacities of CLDHs for Ni and P. All experiments were
117 performed in 250 ml conical flasks and shaken in a temperature controlled orbital
118 shaker (stirring speed of 100 rpm/min) at different temperatures. Constant mass 0.05 g
119 of CLDHs was added to diluting solution (100 mL) with different initial
120 concentrations of Ni and P. Initial pH values of solutions were not adjusted in order to
121 avoid other new ions affecting Ni or P uptake. After a period of time, 2 mL of
122 supernatant was taken and filtered by 0.22 μm membrane. The residual Ni
123 concentration was measured by flame atomic absorption spectrophotometer. For P, it
124 was obtained by the molybdenum-blue ascorbic acid method by UV-visible
125 spectrophotometer at a wavelength of 700 nm[19] .

126 The removal percentage of Ni or P onto CLDHs was calculated according to Eq.
127 (2):[20]

128 $$\text{Removal}\ (\%) = 100\ (C_o - C_t) / C_o \qquad (2)$$

129 Ni or P adsorbed by CLDHs was calculated by the following equation:

130 $$q_t = (C_o - C_e)V/m \qquad (3)$$

131 where C_o, C_t and C_e are initial, time t and equilibrium concentration of Ni or P
132 (mg/L); q_t is adsorptive capacity of adsorbent at time t (mg/g), $q_e = q_t$ when adsorption
133 reaches equilibrium; V is the volume of solution (L) ; m is the mass of adsorbent (g).

2.3.1. Kinetic study

In order to find out the adsorption equilibrium time, different time intervals ranging from 0 to 600 min were set to test at 25, 35, 45 or 55 °C. The kinetics models were adopted during 300 min at 35 and 45 °C. To investigate Ni and P, the reaction solutions were obtained by diluting stock solution 125 times (20.00 mg/L Ni+ 1600 mg/L P) and 1000 times (200.0 mg/L P + 2.500 mg/L Ni), respectively.

2.3.2. Isotherm study

The adsorption isotherms were investigated with a range of different initial concentrations of Ni and P at 25, 35, 45 and 55 °C. The reaction solutions were prepared as follows: (1) Ni (15.00 to 25.00 mg/L) +P (1200 to 2000 mg/L), (2) Ni (0.6300 to 7.500 mg/L) + P (50.00 to 600.0 mg/L). Experiments were carried out for a period of 300 min to allow the uptake of Ni or P up to equilibrium.

2.3.3. Effect of initial ions concentration

The effect of initial Ni or P concentration was studied for 5 h with diluting stock solutions as different proportions at 55 °C. The solutions were prepared as follows: (1) Ni (5.000 to 32.50 mg/L) + P (400.0 to 2600 mg/L), (2) Ni (0.2500 to 37.50 mg/L) + P (20.00 to 3000 mg/L).

2.3.4. Effect of pH

The study was performed at 35 °C for 5 h with different dilution solutions: (1) 20.00 mg/L Ni + 1600 mg/L P (dilution rate of 125 times), (2) 2.500 mg/L Ni + 200.0 mg/L P (dilution rate of 1000 times), (3) 0.250 mg/L Ni + 20.00 mg/L P times (dilution rate of 10000 times). The pH value was determined by PHS-3C meter at different time

156 interval (0 to 300 min).

157 **2.4. Characterization of samples before and after the adsorption**

158 Powder X-ray diffraction (XRD) data were collected with a Rigaku D/MAX-RA
159 instrument using Cu Kα radiation (λ = 0.154184 nm) at 40 kV and 50 mA . Fourier
160 transform infrared spectra (FTIR) were recorded on an AVATAR 370 spectrometer in
161 the 4000–400 cm^{-1} wavenumber range with the KBr disk method. Scanning Electron
162 Microscopy (SEM) images with electron dispersive X-ray analysis (EDX) were taken
163 on the Hitachi S-4800 microscope with EDAX apparatus. The X-ray photoelectron
164 spectroscopy (XPS) was obtained using ESCALAB 250 spectrometer (ThermoFisher
165 Scientific) with an Al Kα X-ray source (0.60 eV) and the optimal energy resolution is
166 less than 0.45 eV.

167 # 3. Results and discussion

168 **3.1. Effect of contact time**

169 The effect of contact time on the adsorption of Ni and P on CLDHs was evaluated to
170 determine the equilibration time and investigate the adsorption process. Plots of Ni or
171 P removal rate versus the change in contact time (0–600 min) at different temperatures
172 were presented in Fig.1. Roughly, there was a monotonic increase in the removal
173 efficiency of Ni or P on CLDHs with time for all temperatures until the adsorption
174 saturation. The removal efficiency of Ni or P on CLDHs increased with increasing
175 temperature at the same contact time. The uptake rate of Ni or P was rapid
176 considerably during starting stage and then suffered a slow process, suggesting one
177 adsorption process not solely controlled by external mass transfer adsorption process

[21]. The changes of Ni or P removal rates from 300 to 600 min were slight, thus the adsorption capacity of CLDHs was basically represented at first 300 min. These also indicated the adsorption of Ni or P on CLDHs was limited and irreversible. Hence, a contact time of 300 min was applied for further studies as adsorption equilibrium time.

3.2. Adsorption kinetics

To determine rate constants and explore the adsorption mechanism of Ni or P on CLDHs, kinetics studies were performed during 300 min. The experimental data were modeled with pseudo-first-order,[22] pseudo-second-order[23] and intraparticle diffusion [24] models, which can be described by the linearized form, respectively:

$$\ln (q_e - q_t) = \ln q_e - k_1 t \quad (4)$$

$$t/q_t = 1/k_2 q_e^2 + t/q_e \quad (5)$$

$$q_t = k_i t^{0.5} \quad (6)$$

where k_1 (/min), k_2 (g/(mg min)) and k_i (mg/(g $min^{0.5}$)) are the rate constants of pseudo-first-order , pseudo-second-order and intraparticle diffusion models. Relevant kinetics parameters calculated from the slopes and intercepts of linear plots, were presented in Table 1.

In Table 1, the equilibrium adsorption capacities ($q_{e,cal}$) of the pseudo-second-order model were close to the experimental results ($q_{e,exp}$) at high correlation coefficients R^2 (>0.99) compared to the other two models. Consistent result could be obtained from Fig.3, where the fitting curves of the pseudo-second-order model were presented. Herein, the pseudo-second-order model could fairly well describe the

uptake of Ni and P onto CLDHs, revealing the chemical sorption process.[25] Additionally, the rate constant K_2 and equilibrium capacity $q_{e,cal}$ for Ni or P increased with increasing temperatures, demonstrating that raising temperatures were favorable to adsorption progresses.

3.3. Effect of ion initial concentration

The removal performance of CLDHs for Ni or P was shown in Fig.2 as a function of initial ion concentration. Fig.1 showed the adsorption equilibrium could reach within 300 min, thus the contact time was set to 300 min. It can be seen from Fig.2 that increased initial ions concentrations would result in reduction in removal efficiencies of Ni and P. In terms of Ni, it could be effectively removed from solutions with an initial concentration lower than 10.00 mg/L. Likewise, as the initial concentration of P was under 20.00 mg/L, the removal efficiency remained above 90%. Moreover, the removal efficiency turned lower than 50% as the initial concentrations of Ni and P went higher than 25.00 mg/L and 400.00 mg/L, respectively. Therefore, the initial concentrations of Ni (20.00 mg/L) and P (200.00 mg/L), where the approximate removal efficiency (over 50%) could be obtained, were chosen for kinetic study.

As seen in Fig.2, with increasing initial concentration, the adsorption amounts of Ni firstly rose and then dropped, while the adsorption quantity of P strictly increased. With the same dilution ratio of stock solutions, the adsorption quantity of CLDHs for P was much higher comparing with Ni, elucidating higher affinity of CLDHs for P than for Ni. The co-existing high concentration P might have a negative effect on Ni removal. Considering the appropriate removal efficiency and adsorption capacity,

initial concentration of Ni and P ranged were 15.00-25.00 mg/L and 50.00-600.00 mg/L, respectively, which were applied in adsorption isotherm study.

3.4. Adsorption isotherm

Adsorption isotherm is usually applied in describing the interaction between adsorbents and adsorbates, and evaluate the adsorption capacity of adsorbents.[26] Freundlich and Langmuir isotherm models were most frequently applied for analyzing equilibrium sorption data.

The Langmuir isotherm model assumes that the adsorbed layer is monolayer and all adsorption sites are equal and homogeneous.[27] The equation can be given as follows:[28]

$$C_e/q_e=1/(q_m K_{L)} +C_e/q_m \quad (7)$$

where q_m (mg/g) is the maximum adsorption capacity; K_L (L/mg) is the Langmuir constant related to the energy of adsorption.

The Freundlich model based on the assumption that a multilayer sorption occurs on heterogeneous surface sites with different bond energies.[29] The liner equation of Freundlich model can be expressed as follows:

$$\ln q_e = \ln K_F +1/n \ln C_e \quad (8)$$

where K_F (mg/g)·(L/mg)^n and n are Freundlich constants related to adsorption intensity.

Adsorption isotherms of Ni or P on CLDHs were fitted with Langmuir and Freundlich models at various temperatures, as shown in Fig. 4. The parameters of two models were summarized in Table 2. Obviously, for Ni adsorption, the correlation

coefficient (R^2) values all exceed 0.99 derived from Langmuir model, suggesting Langmuir model could better describe Ni adsorption than Freundlich model. Whereas the Freundlich model was more properly attributing to the higher R^2 of Freundlich model than those of Langmuir model in case of P adsorption. It concluded that the adsorption process of Ni was homogeneous, while P was heterogeneous.

In Fig. 4, the adsorption capacity of CLDHs was improved with increasing equilibrium concentrations of Ni or P attributing to the ascending initial concentrations. The rising temperatures also promoted the adsorption capacity of CLDHs for Ni or P, which was consistent with kinetics study. Therefore, the maximum adsorption quantity could be obtained at 55 °C with maximal initial concentrations of 25.00 (Ni) and 600.0 (P) mg/L, respectively. The adsorption capacity of CLDHs was 22.87 mg/g for Ni based on Langmuir model and 761.5 mg/g for P based on Freundlich model.

The sorption capacity of Ni or P on CLDHs was compared with some other adsorbents and was summarized on Table 3.[6, 16, 19, 30-37] On the basis of the results, hydroxides have higher adsorption capacity for Ni or P than other adsorbents, but calcined hydroxides possessed higher superiority than LDHs in single ion adsorption system. It indicated CLDHs was a kind of potential adsorbents for Ni and P removal. The sorption capacity of Ni on CLDHs dropped in present study (22.87 mg/g) comparing the single ion adsorption system (361.1 mg/g).[34] However, P went up. It also indicated that the co-existing high concentration P had a negative influence on the uptake of Ni removal, as the effect of ion initial concentration results shows.

3.5. Effect of temperature

The plots of q_t versus t (Fig.3) and q_e versus C_e (Fig.4) at varying temperatures implied that the increased temperatures promoted Ni or P removal. It could be speculated that the uptake of Ni or P on CLDHs was endothermic with more active sites of adsorbent surfaces at higher temperatures.

In order to further understand the effect of temperature, thermodynamic parameters including the change in the Gibbs free energy (ΔG^o, J/mol), enthalpy (ΔH^o, J/mol) and entropy (ΔS^o, J/mol K) were analyzed. These parameters can provide in-depth information regarding the inherent energy and structural changes, and contribute to evaluate the orientation and feasibility of the adsorption reaction.[38] Thermodynamic equations can be expressed as follows:[30]

$$\Delta G^\circ = - RT \ln K_D \quad (9)$$

$$\Delta G^\circ = \Delta H^\circ - T\Delta S^\circ \quad (10)$$

$$\ln K_D = \Delta S^\circ/R - \Delta H^\circ/RT \quad (11)$$

where R is the universal gas constant (8.314×10^{-3} kJ/mol K); T is the absolute temperature (K); K_D is the adsorbate distribution coefficient and is calculated by Eq. (9),

$$K_D = q_e / C_e \quad (12)$$

The values of thermodynamics parameters reported in Table 4 were obtained from the linear plot of lnK versus 1/T (Fig.5). Obviously, the values of ΔH° and ΔS° were positive, and the value of ΔG° was negative for all the experiments. The positive ΔH° implied that the endodermic nature of the adsorption process [16], thus, with rising

temperatures, the adsorption capacity and adsorption rate of CLDHs for Ni or P improved. The positive value of ΔS° showed the increased randomness ascribing to the shift of partial adsorbates from solutions to adsorbent-solution interfaces during adsorption processes. Hence, the concentration of Ni or P in solution decreased with the increased time and temperature. With a rise of temperature, the negative ΔG° decreased, suggesting the spontaneous adsorption process. And the increased temperature was favorable for Ni or P adsorption, which was in accordance with previous studies.

3.6. Effect of pH

The pH value could affect the chemical properties of adsorbents and adsorbates, thereby influencing the adsorption process of Ni or P on CLDHs. As illustrated in Fig.6, with increasing time, pH values dramatically increased at the beginning, followed by slow increasing before near balance condition, which was consistent with the results of Fig.1 and Fig.3, suggesting that pH variation affected the removal of Ni or P owing to the released hydroxyls (OH^-) of adsorbents. In adsorption processes, pH values within the range of 5-10 were low 12.5 (pH_{PZC} of Mg_3Al CLDHs),[39] implying the positive charges of adsorbents surfaces. CLDHs could occur to rehydration in solutions leading to the release of OH^- with increased pH. Herein, plentiful OH^- were produced on the surfaces of adsorbents and partially transferred to solutions, causing rising alkalinity gradients from liquid phases to solid-liquid interfaces. Under the effect of alkalinity gradient, Ni was easily transferred from liquid phases to solid-liquid interfaces in the form of hydroxides. Simultaneously, anions of solutions

could gather towards positively charged surfaces of adsorbents in electrostatic attraction. Ionic pollutants escaped from solutions to adsorbents surfaces purifying the wastewater. Because of the "memory effect",[14] Ni could occupy sites of Mg in sheets and participate in refactoring lattices of LDHs with isomorphic substitution,[34, 40] anions could concomitantly incorporate into interlayers with the electrostatic attraction.

Additionally, phosphorus mainly existed in the form of $H_2PO_3^-$ (with few $H_2PO_2^-$) in the electroless nickel plating wastewater. The dissociation equilibrium of H_3PO_3 or H_3PO_2 in aqueous solution is pH-related, which can be presented as:

$$H_3PO_3 \rightleftharpoons H_2PO_3^- + H,\ pK_a=1.3 \quad (13)$$

$$H_2PO_3^- \rightleftharpoons HPO_3^{2-} + H^+,\ pK_a=6.6 \quad (14)$$

$$H_3PO_2 \rightleftharpoons H_2PO_2^- + H^+,\ pK_a=11 \quad (15)$$

In Fig. 6(b) and (c), the pH values basically changed in the range of 5-7. Herein, plentiful $H_2PO_3^-$ (with few $H_2PO_2^-$) was the dominant species in adsorption processes. The affinities of LDHs were in the sequence $H_2PO_3^-/H_2PO_2^- > CO_3^{2-} > SO_4^{2-} > OH^-$/ lactic acid/acetic acid [41, 42], thus phosphorus could be firstly removed from solutions and gathered at the surfaces of adsorbents with electrostatic attraction.

3.7. Characterization

Fig.7 represented XRD patterns of Mg-Al-CO_3 LDHs, CLDHs, CLDHs after adsorption of Ni and P with low initial concentration ([Ni + P] =0.2500 mg/L + 20.00 mg/L) (R_1-CLDHs), and CLDHs after adsorption of Ni and P with high initial concentration ([Ni + P]) =20 mg/L + 1600 mg/L) (R_2-CLDHs). The X-ray patterns of

LDHs demonstrated not only sharp and symmetrical peaks (003, 006, 110 and 113), but some other asymmetrical peaks of hydrotalcites structures as well, indicating a well-crystallized LDHs. Moreover, a hexagonal lattice with an R3m rhombohedral symmetry could be indexed through the patterns of LDHs, which could further prove the successful synthesis of hydroxides materials. The peaks of hydrotalcites structures disappeared in the XRD patterns of CLDHs, indicating that the calcinations intensely destroyed original hydrotalcites structures resulting in the collapse of sheets structures and the formation of a mixed oxide Mg(Al)O with MgO-periclase structures (JCPDS 45-0496).[43, 44] The patterns of R_1-CLDHs were similar to patterns of LDHs with decreasing relative intensities of peaks, inferring the formation of hydrotalcites after adsorption. It might show that Ni indeed incorporated into hydrotalcites lattices. It was interested that the 2θ of characteristic diffraction peak (003) were similar in Fig.6 (a) and Fig.6 (b), revealing the interlayer spacing not changed after adsorbing $H_2PO_3^-$ or $H_2PO_2^-$. Therefore, it might be reasonable explanation that the adsorbed phosphorous ions were mainly utilized by the superficial sheets of the reconstructed LDHs, and many OH^-, CO_3^{2-} or SO_4^{2-} inserted into the interlayers of internal sheets. While the patterns of R_2-CLDHs contained some unobvious peaks attributing to the low crystallinity, which was different from the patterns of LDHs indicating non-layer structures of R_2-CLDHs. It was reasonable to speculate that a large amount of $H_2PO_3^-$ (or $H_2PO_2^-$) in solutions affected the reconstructions of LDHs structures, forming new adsorption products. Without LDHs structures, Ni could not be incorporated into hydrotalcites lattices, inducing decreased adsorption capacity. It was indicated that Ni

uptake was affected by the presence of plentiful P as the effect of initial ion concentration results shows. Besides, via the JCPDS database, the $MgHPO_3$ phase (JCPDS 72-1173) was observed for R_2-CLDHs sample. The HPO_3^{2-} generated attribute to the release of abundant OH^- leading to hydrolysis reaction of $H_2PO_3^-$. The low crystallinity showed that the adsorption products in high concentration solutions were mixtures. Combining the results of pH effect, the mixtures mainly contained metal (Mg, Al or Ni) salts of phosphites, hypophosphites, hydroxides.

FTIR analysis can provide direct information about surface and bulk species.[45] The FTIR spectra of LDHs, CLDHs, R_1-CLDHs and R_2-CLDHs were illustrated in Fig.7. Broad bands in the range of 3400 – 3500 cm^{-1} (O–H stretching vibration) and weak bands at about 1600 cm^{-1} (O–H bending vibration) demonstrated the presence of interlaminar water molecules.[46] All the spectra contained a strong bond at about 1400 cm^{-1}, attributing to the asymmetric stretching vibration of CO_3^{2-} of interlayers. The peaks between 400 and 700 cm^{-1} were assigned to metal–oxygen–metal stretching [47]. After adsorption of Ni and P, the new bands appeared at about 790 and 1120 cm^{-1}in Fig.6 (b) and (c), which might be indicative of Ni–O stretching and P–O vibration, respectively.[48] These indicated CLDHs could indeed simultaneously adsorb Ni and P.

In order to further investigate the adsorption mechanism of Ni or P, the morphology of LDHs, CLDHs, R_1-CLDHs and R_2-CLDHs and some corresponding chemical compositions were presented in Fig. 8. The SEM images showed the alveolate-like morphology with plentiful flakiness for LDHs, displaying the thin crystals of LDHs.[49] It can be further observed in Fig. 8 (b) that, the flakiness

structures existed were aggregative and rough without abundant morphologies, showing the collapsed layer structures of CLDHs by calcinations. In addition, the morphology of R_1-CLDHs was similar to LDHs, and EDX spectrums were presented for the components of LDHs (C, H, O, Mg and Al) and adsorbates (Ni and P). With low contents of Ni and P, it was observed that the layered structures of hydrotalcites was reconstructed via isomorphous substituting Mg with Ni, utilizing $H_2PO_3^-$/ $H_2PO_2^-$ to balance the positive charges of superficial sheets and intercalating OH^-, CO_3^{2-} or SO_4^{2-} into interlayers of internal sheets according to the XRD results. In high concentration solutions, more Ni and P could be absorbed by CLDHs, as indicated by the EDX spectrums of R_1-CLDHs and R_2-CLDHs. However, the SEM image of R_2-CLDHs was without obvious alveolate-like morphology and was evidently different from that of LDHs or R_1-CLDHs, which showed on the morphology that new adsorption products were generated and did not belong to LDHs. This was in accordance with the results of XRD.

XPS technique was employed for in-depth analysis of adsorption processes. Fig.9 (a) shows the surface compositions of LDHs, R_1-CLDHs, R_2-CLDHs and CLDHs. The carbon, oxygen, Mg and Al could be observed in all spectra. New peaks of Ni2p and P2p on R_1-CLDHs or R_2-CLDHs could be detected, revealing Ni or P adsorption on CLDHs. Specifically, there was not obvious peak for Ni2p on R_1-CLDHs, indicating low adsorption quantity due to low initial concentration of Ni. In Fig.9 (b), the main contribution of Ni 2p core level spectrum was centered at 856.8 eV, which was assigned to Ni^{2+} interacting possibly with $H_2PO_3^-$ or $H_2PO_2^-$. [50, 51] Regarding to P

2p, two deconvoluted peaks appeared after adsorption, verifying P existed in the spent EN plating wastewater in two forms of $H_2PO_3^-$ and $H_2PO_2^-$.[50, 52] Obviously, the peak, centered at high binding energy side, predominantly ascribe the high proportion of $H_2PO_3^-$ in total phosphorus content. Besides, P still existed in the original valence state after adsorption, which implied that they were used to balance the positive charges of produced sheets during CLDHs refactoring processes and the adsorbed contents of P not enough to changed LDHs structures. Two peaks of R_2-CLDHs upward shifted compared to R_1-CLDHs, indicating the change of the bonding environment of $H_2PO_3^-$ or $H_2PO_2^-$ species. Mg_3Al CLDHs, one kind of mixed metal oxide (Mg (Al) O), when contacted solutions, they could form Mg or Al hydroxides on the surfaces, occur to ionization effect together with Ni hydroxides of the surfaces, and generate the single octahedral sheets[53]. According to the multilayer sorption obtained from Freundlich model, large quantities of $H_2PO_3^-$or $H_2PO_2^-$ on the surfaces of adsorbents prior occupied the adsorption sites of surface sheets and interlayers by linking the generated single sheets, and excess parts replaced the sites of –OH of sheets. Most of $H_2PO_3^-$or $H_2PO_2^-$ incorporated into interlayers causing sheets distortions, and sheets could not stack together forming LDHs structures. Because abundant OH^- releasing by adsorbents surfaces and large quantities of $H_2PO_3^-$or $H_2PO_2^-$ on the surfaces of adsorbents existed, finally they could combine with ionized Mg^{2+}, Al^{3+} or Ni^{2+} formed metal salts. These results are in accordance with the XRD and SEM.

3.8. Adsorption mechanism

Based on the above studies, the adsorption mechanisms could be speculated as

follows: (1) for low concentration solutions, CLDHs took place rehydration and rebuilt LDHs structures. Most Ni was incorporated into sheets and P was mainly utilized to balance the positive charges of superficial sheets; (2) for high concentration solutions, firstly, Ni adhered to surfaces of adsorbents via alkalinity gradient in the form of hydroxide precipitations, and P accumulated on positively charged adsorbent surfaces through electrostatic attraction. Then, abundant $H_2PO_3^-$ or $H_2PO_2^-$ occupied the sites of interlayers and replaced the sites of –OH of sheets, leading to twisty sheets and affecting the formation of LDHs structures. Finally mixed metal (Mg, Al or Ni) salts of phosphites, hydroxides or hypophosphites were produced. These reactions might be expresses as Eq. (16)-(17), and were depicted in Scheme 1.

$$Mg_{1-x}Al_x\,O_{1+x/2} + yNi^{2+} + (x+2y)\,H_2PO_3^-/H_2PO_2^- + (m+1+x/2)\,H_2O \longrightarrow$$

$$Mg_{1-x}Ni_yAl_x\,(OH)_2\,H_2PO_3^-/H_2PO_2^-{}_{(x+2y)} \cdot mH_2O + xOH^- \quad (16)$$

$$Mg(Al)O + Ni^{2+} + H_2PO_3^-/H_2PO_2^- + H_2O + CO_2 \longrightarrow$$

$$(Mg/Al/Ni)(H_2PO_3/H_2PO_2)_n + (Mg/Al/Ni)(OH)_n + (Mg/Al/Ni)_2(CO_3)_n + OH^- \quad (17)$$

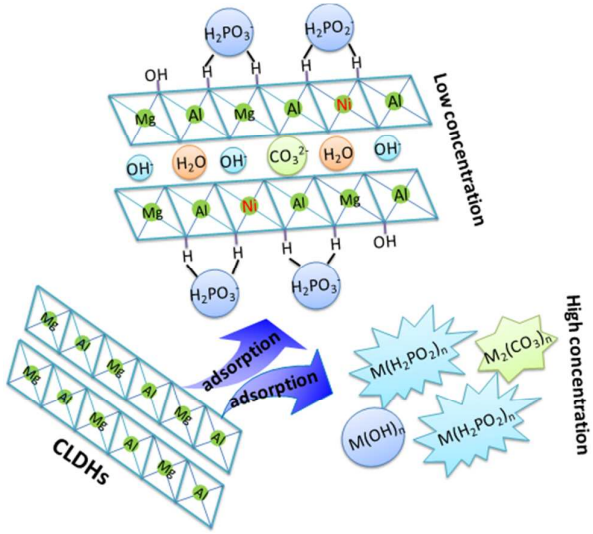

Scheme 1. Schematic representation of probable adsorption mechanisms.

4. Conclusions

The CLDHs demonstrated excellent purification effect for spent EN plating wastewater with respect to co-removal of nickel and phosphorus. It was found that the adsorption process of Ni and P on CLDHs was endothermic and spontaneous, together with increasing randomness of the system. Pseudo-second-order equation well explained the kinetic data and revealed the possibility of chemisorptions. Moreover, adsorption isotherms could be fitted by Langmuir and Freundlich model, showing different uptake processes of Ni and P. As a result, CLDHs could rebuild hydrotalcites structures utilizing the ions of Ni and P in low concentration solutions, while new mixed metal salts were generated in high concentration solutions. Additionally, the removal of Ni was negatively impacted, because of the adsorption of large amounts of P. This study demonstrated that CLDHs possessed vast application potential in treating spent EN plating wastewater with high efficiency, easy operation and low cost.

Acknowledgments

The current work was financially supported by Science and Technology Development Plan of Shandong Province of China (No.2012GGE27098) and Independent Innovation Projects of Important Key Technology, Shandong Province (No. 2014GJJS0501).

References

1. S. Tengsuwan and M. Ohshima, J. Supercrit. Fluids, 2012, **69**, 117-123.

2. T. Zhai, X. Lu, G. Cui, G. Wu, J. Qu and Y. Tong, *J. Mater. Chem. C*, 2013, **1**,

458 5149.

459 3. Y. J. Shih, C. P. Lin and Y. H. Huang, *Sep. Purif. Technol.*, 2013, **104**,
460 100-105.

461 4. M. Jiang, X. Jin, X. Lu and Z. Chen, *Desalination*, 2010, **252**, 33-39.

462 5. K. Dermentzis, *J. Hazard. Mater.* , 2010, **173**, 647-652.

463 6. Y. Tu and C. You, *Chem. Eng. J.*, 2014, **251**, 285-292.

464 7. M. Hunsom, K. Pruksathorn, S. Damronglerd, H. Vergnes and P. Duverneuil,
465 *Water Res.*, 2005, **39**, 610-616.

466 8. Y. Huang and M. Tanaka, *J. Hazard. Mater.* , 2009, **164**, 1228-1235.

467 9. Xiaoya Yuan, Jian Wang, Chao Zhou, Qi Tang, Xiaobei Rao, *Chem. Eng. J.*,
468 2013, **221**, 204–213.

469 10. T. Kwon, G. A. Tsigdinos and T. J. Pinnavaia, *J. Am. Chem. Soc.*, 1988, **110**,
470 3653-3654.

471 11. J. Zhou, Y. Wu, C. Liu, A. Orpe, Q. Liu, Z. Xu, G. Qian, S. Qiao, *Environ. Sci.*
472 *Technol*, 2010, **44**, 8884–8890.

473 12. Y. Xu, J. Zhang, J. Zhou, C. Chen, Q. Liu, G. Qian and Z. P. Xu, *Chem. Eng.*
474 *J.*, 2013, **215-216**, 411-417.

475 13. Y. Xu, J. Zhang, J. Zhou, C. Chen, Q. Liu, G. Qian, Z. Xu, J. Environ. Chem.
476 Eng., 2015, DOI: 10.1016/j.jece.2015.03.017.

477 14. O. D. Pavel, R. Bîrjega, M. Che , G. Costentin, E. Angelescu, S. Serban., Catal.
478 Commun., 2008, **9**, 1974–1978.

479 15. K. H. Goh, T. T. Lim and Z. Dong, *Water Res.*, 2008, **42**, 1343-1368.

16. X. Liang, Y. Zang, Y. Xu, X. Tan, W. Hou, L. Wang and Y. Sun, Colloids. Surf. A Physicochem. Eng. Asp., 2013, **433**, 122-131.

17. L. Fang, W. Li, H. Chen, F. Xiao, L. Huang, P. E. Holm, H. C. B. Hansen and D. Wang, *RSC Adv.*, 2015, **5**, 18866-18874.

18. T. Kameda, M. Umetsu and T. Yoshioka, *New J. Chem.*, 2015, **39**, 4078-4085.

19. P. Cai, H. Zheng, C. Wang, H. Ma, J. Hu, Y. Pu and P. Liang, *J. Hazard. Mater.*, 2012, **213-214**, 100-108.

20. R. Wang, T. Wen, X. Wu and A. Xu, *RSC Advances*, 2014, **4**, 21802.

21. Y. Li, Q. Yue and B. Gao, *J. Hazard. Mater.*, 2010, **178**, 455-461.

22. K. K. C. Namasivayam, *Carbon*, 1999, **37**, 79–84.

23. Y. S. Ho, G Mckay, *Process Biochemistry*, 1999, **34**, 451–465.

24. M. Jansson-Charrier, E. Guibal, J. Roussy, B. Delanghe, P. Le Cloirec, *Wat. Res.*, 1996, **30**, 465--475.

25. D. Wan, H. Liu, R. Liu, J. Qu, S. Li and J. Zhang, *Chem. Eng. J.*, 2012, **195-196**, 241-247.

26. Z. Zhang, M. Liao, H. Zeng, S. Xu, X. Liu, J. Du, P. Zhu, Q. Huang, *Appl. Clay Sci.* , 2014, **102**, 246-253.

27. J. C. T. H. Genc-Fuhrman, D. McConchie, *Environ. Sci. Technol.*, 2004, **38**, 2428–2434.

28. I. Langmuir, *J. Am. Chem. Soc.*, 1916, **38**, 2221–2295.

29. Y. Cengeloglu, A. Tor, M. Ersoz, G. Arslan., *Sep. Purif. Technol.*, 2006, **51**, 374-378.

30. M. G. Vieira, A. F. Neto, M. L. Gimenes and M. G. da Silva, *J. Hazard. Mater.*, 2010, **177**, 362-371.

31. M. El-Sadaawy and O. Abdelwahab, Alex. Eng. J., 2014, **53**, 399-408.

32. N. T. Abdel-Ghani, G. A. El-Chaghaby and F. S. Helal, J. Adv. Res., 2014, DOI: 10.1016/j.jare.2014.06.001.

33. C. Jeon, J. Cha, J. Ind. Eng. Chem., 2014, DOI: 10.1016/j.jiec.2014.09.016.

34. M. Sun, Y. Xiao, L. Zhang, X. Gao, W. Yan, D. Wang and J. Su, *Chem. Eng. J.*, 2015, **272**, 17-27.

35. J. Xie, Y. Lin, C. Li, D. Wu and H. Kong, Powder Technol., 2015, **269**, 351-357.

36. M. Zamparas, M. Drosos, Y. Georgiou, Y. Deligiannakis and I. Zacharias, *Chem. Eng. J.*, 2013, **225**, 43-51.

37. J. Zhou, S. Yang, J. Yu and Z. Shu, *J. Hazard. Mater.*, 2011, **192**, 1114-1121.

38. A. Ş. Yargıç, R. Z. Yarbay Şahin, N. Özbay and E. Önal, J. Clean. Prod., 2015, **88**, 152-159.

39. L. Xiao, W. Ma, M. Han and Z. Cheng, *J. Hazard. Mater.*, 2011, **186**, 690-698.

40. T. H. Kim, W. J. Lee, J. Y. Lee, S. M. Paek and J. M. Oh, Dalton T., 2014, **43**, 10430-10437.

41. S. Miyata, Clay. Clay Miner.,1983, **31**, 305-311.

42. T. Wu, L. Mao and H. Wang, *RSC Adv.*, 2015, **5**, 23246-23254.

43. D. Lan, L. Ma, Y. Chun, C. Wu, L. Sun and J. Zhu, J. Catal., 2010, **275**, 257-269.

44. M. Hájek, P. Kutálek, L. Smoláková, I. Troppová, L. Čapek, D. Kubička, J. Kocík and D. N. Thanh, *Chem. Eng. J.*, 2015, **263**, 160-167.

45. T. Wang, Z. Cheng, B. Wang and W. Ma, *Chem. Eng. J.*, 2012, **181-182**, 182-188.

46. R. Shan, L. Yan, Y. Yang, K. Yang, S. Yu, H. Yu, B. Zhu, B. Du, J. Ind. Eng. Chem., 2015, **21**, 561-568.

47. H. Zaghouane-Boudiaf, M. Boutahala and L. Arab, *Chem. Eng. J.*, 2012, **187**, 142-149.

48. Q. Yu, Y. Zheng, Y. Wang, L. Shen, H. Wang, Y. Zheng, N. He and Q. Li, *Chem. Eng. J.*, 2015, **260**, 809-817.

49. Q. Guo and E. J. Reardon, *Appl. Clay Sci.* , 2012, **56**, 7-15.

50. J. A. Cecilia, A. Infantes-Molina, E. Rodríguez-Castellón, A. Jiménez-López, J. Catal., 2009, **263**, 4-15.

51. N. Escalona, J. Ojeda, P. Baeza, R. García, J. M. Palacios, J. L. G. Fierro, A. L. Agudo and F. J. Gil–Llambías, Appl. Catal. A Gen. 2005, **287**, 47-53.

52. H. Song, M. Dai, H. Song, X. Wan and X. Xu, *A* Appl. Catal. A Gen., 2013, **462-463**, 247-255.

53. Y. Xiao, M. Sun, L. Zhang, X. Gao, J. Su and H. Zhu, *RSC Adv.*, 2015, **5**, 28369-28378.

Figure

Figures List:

Fig.1. Effect of contact time of Ni or P on CLDHs at different temperatures (a. [Ni + P] =20 mg/L + 1600 mg/L, b. [Ni + P] =2.5 mg/L+ 200 mg/L, [CLDHs] =0.5 g/L).

Fig.2. Effect of initial concentration of Ni (left) or P (light) on the removal efficiency and adsorption capacity ([CLDHs] =0.5 g/L, t=300 min, T=55 °C).

Fig.3. Kinetics of Ni (a) or P (b) adsorption on CLDHs at different temperatures and data fitting by pseudo-first-order, pseudo-second-order and particle diffusion models. (a. [Ni + P] =20 mg/L + 1600 mg/L, b. [Ni + P] =2.5 mg/L+ 200 mg/L, [CLDHs] =0.5 g/L, t=300 min).

Fig.4. Sorption isotherm of Ni (left) or P (right) using CLDHs at 25, 35, 45 or 55 °C. Solid lines and dot lines represent predicted data by the Langmuir model and Freundlich model, respectively, and the symbols are the experimental data ([CLDHs] =0.5 g/L, t=300 min).

Fig.5. Plot of $\ln K_D$ versus 1/T for estimation of thermodynamic parameters for the adsorption of Ni (left) or P (right) on CLDHs.

Fig.6. Effect of pH on the adsorption of Ni and P on CLDHs in different concentrations of dilute solution (a. [Ni + P] =0.25 mg/L + 20 mg/L, b. [Ni + P] =2.5 mg/L+ 200 mg/L, c. [Ni + P] =20 mg/L + 1600 mg/L, [CLDHs] =0.5 g/L, t=300 min, T=35 °C).

Fig.7. XRD patterns (left) and FT-IR (right) for LDHs (a), CLDHs (b), R_1-CLDHs (c)

and R_2-CLDHs (d).

Fig.8. The SEM image of LDHs (a), CLDHs (b), R_1-CLDHs(c) or R_2-CLDHs (d) and the corresponding EDX spectrum of R_1-CLDHs(c) or R_2-CLDHs (d).

Fig.9. (a) X-ray photoelectron spectra of LDHs, R_1-CLDHs, R_2-CLDHs and CLDHs, (b) Ni2p of R_2-CLDHs core level spectrum after adsorption on CLDHs and (c) comparison of the XPS P2p peaks between R_1-CLDHs(c) and R_2-CLDHs.

Figures:

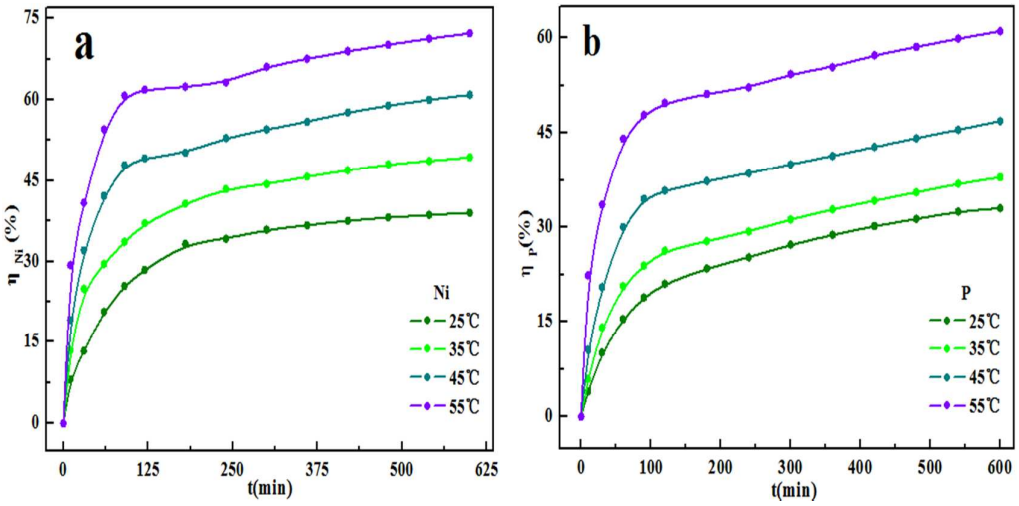

Fig.1. Effect of contact time of Ni (a) or P (b) on CLDHs at different temperatures (a. [Ni + P] =20 mg/L + 1600 mg/L, b. [Ni + P] =2.5 mg/L+ 200 mg/L, [CLDHs] =0.5 g/L).

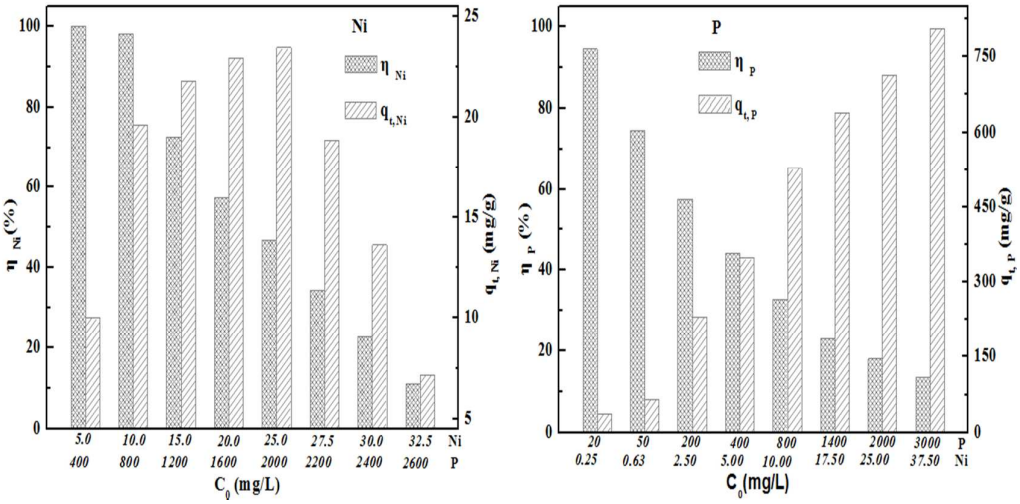

Fig.2. Effect of initial concentration of Ni (left) or P (light) on the removal efficiency and adsorption capacity ([CLDHs] =0.5 g/L, t=300 min, T=55 °C).

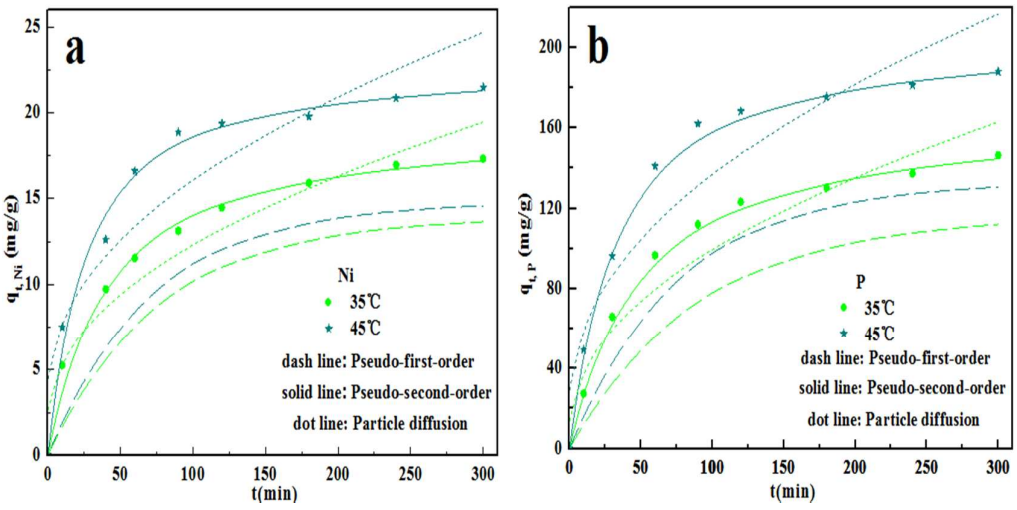

Fig.3. Kinetics of Ni (a) or P (b) adsorption on CLDHs at different temperatures and data fitting by pseudo-first-order, pseudo-second-order and particle diffusion models. (a. [Ni + P] =20 mg/L + 1600 mg/L, b. [Ni + P] =2.5 mg/L+ 200 mg/L, [CLDHs] =0.5 g/L, t=300 min).

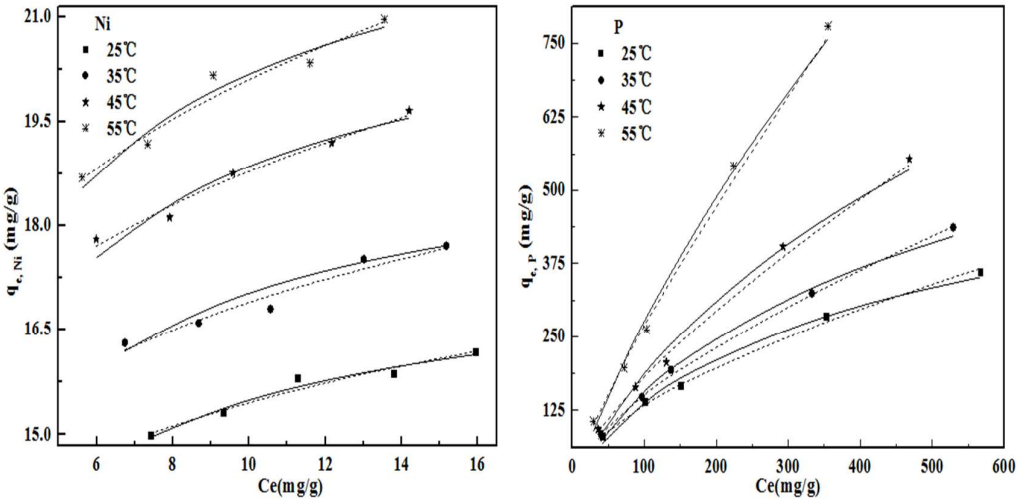

Fig.4. Sorption isotherm of Ni (left) or P (right) using CLDHs at 25, 35, 45 or 55 °C. Solid lines and dot lines represent predicted data by the Langmuir model and Freundlich model, respectively, and the symbols are the experimental data ([CLDHs] =0.5 g/L, t=300 min).

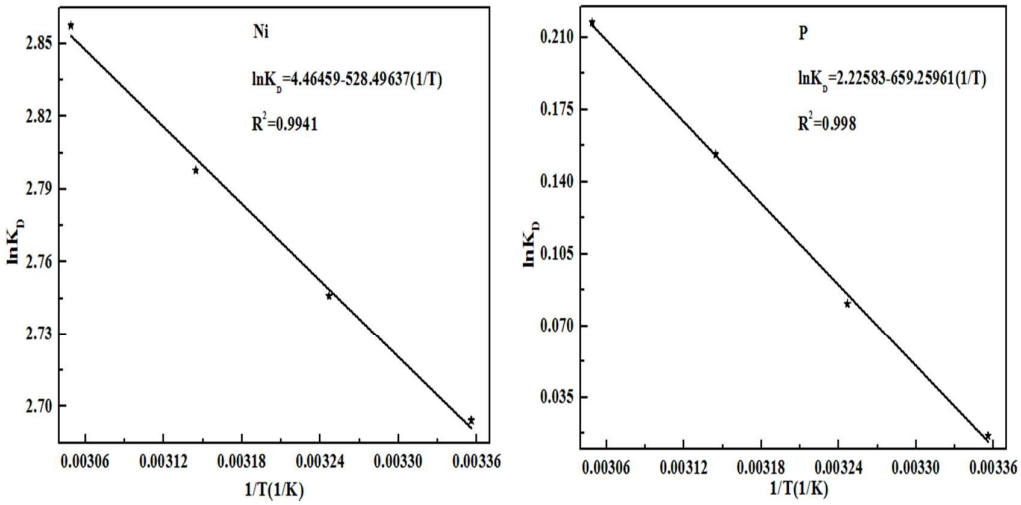

Fig.5. Plot of $\ln K_D$ versus 1/T for estimation of thermodynamic parameters for the adsorption of Ni (left) or P (right) on CLDHs.

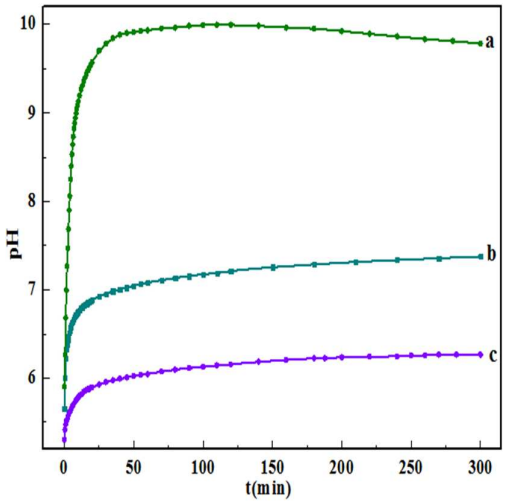

Fig.6. Effect of pH on the adsorption of Ni and P on CLDHs in different concentrations of dilute solution (a. [Ni + P] =0.25 mg/L + 20 mg/L, b. [Ni + P] =2.5 mg/L+ 200 mg/L, c. [Ni + P] =20 mg/L + 1600 mg/L, [CLDHs] =0.5 g/L, t=300 min, T=35 ℃).

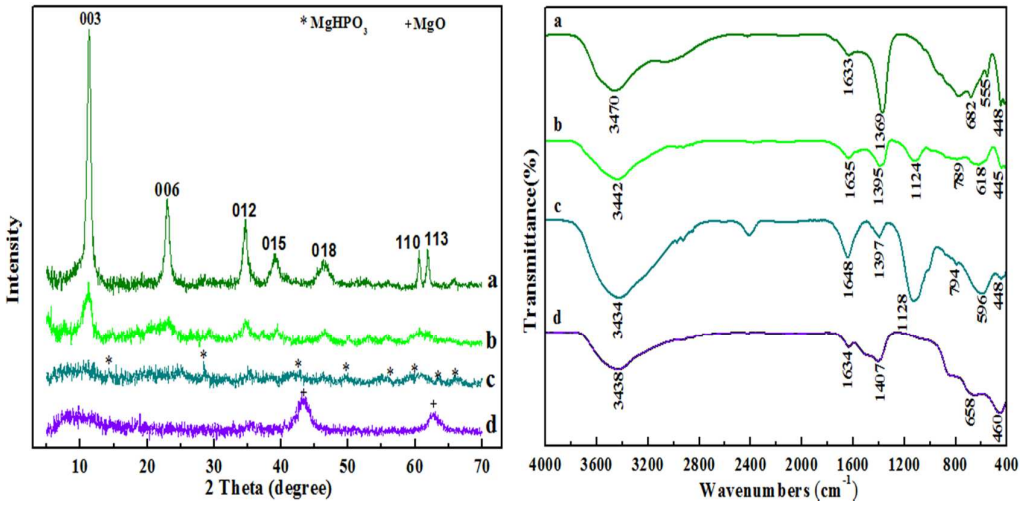

Fig.7. XRD patterns (left) and FTIR (right) for LDHs (a), R_1-CLDHs (b), R_2-CLDHs (c) and CLDHs (d).

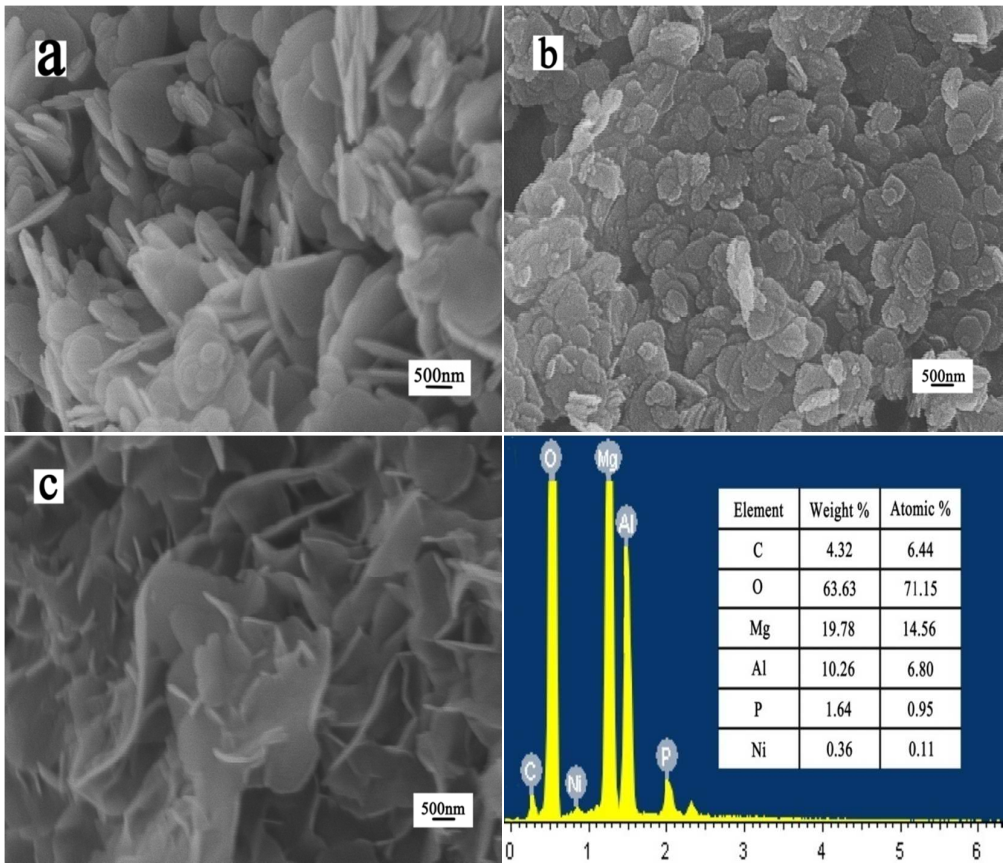

Element	Weight %	Atomic %
C	4.32	6.44
O	63.63	71.15
Mg	19.78	14.56
Al	10.26	6.80
P	1.64	0.95
Ni	0.36	0.11

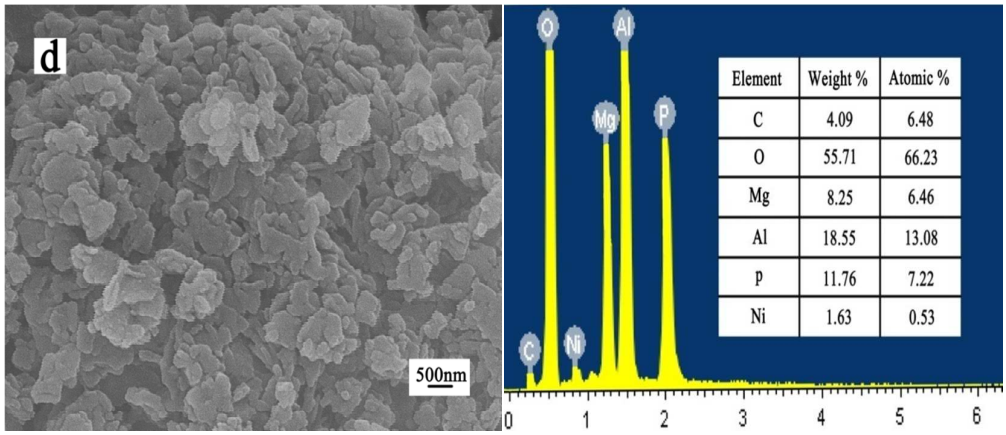

Element	Weight %	Atomic %
C	4.09	6.48
O	55.71	66.23
Mg	8.25	6.46
Al	18.55	13.08
P	11.76	7.22
Ni	1.63	0.53

Fig.8. The SEM image of LDHs (a), CLDHs (b), R_1-CLDHs(c) or R_2-CLDHs (d) and the corresponding EDX spectrum of R_1-CLDHs(c) or R_2-CLDHs (d).

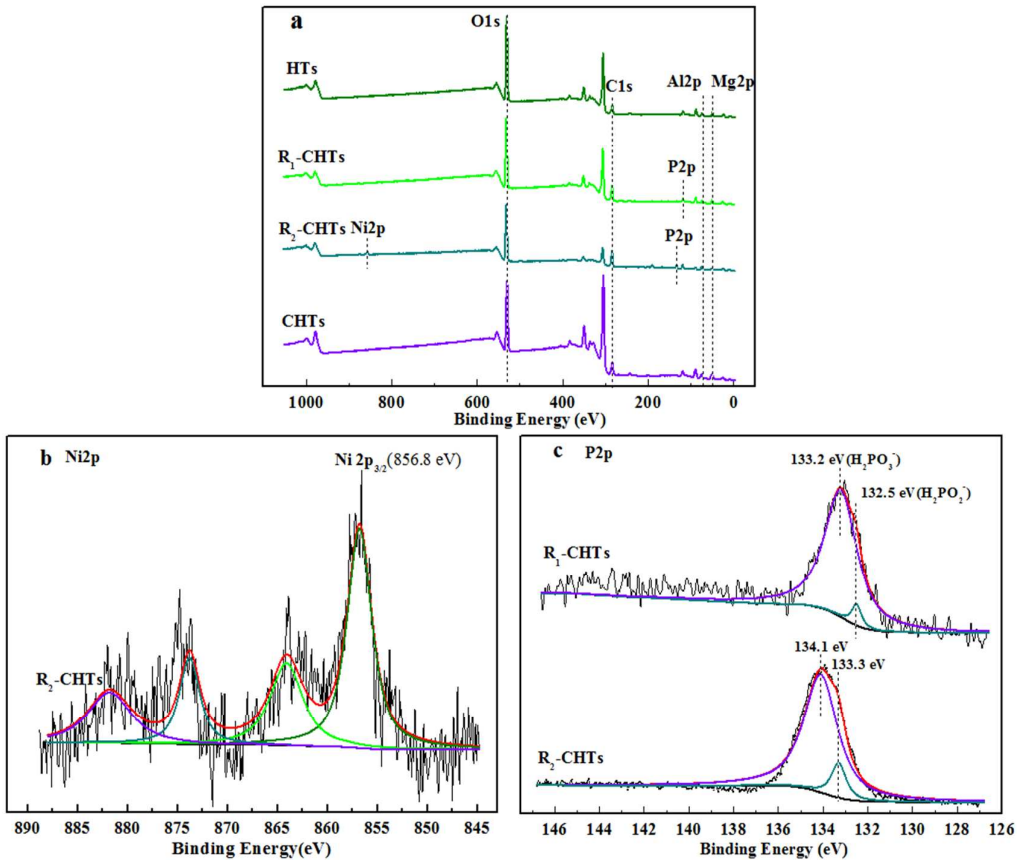

Fig.9. (a) X-ray photoelectron spectra of LDHs, R_1-CLDHs, R_2-CLDHs and CLDHs, (b) Ni2p of R_2-CLDHs core level spectrum after adsorption on CLDHs and (c) comparison of the XPS P2p peaks between R_1-CLDHs(c) and R_2-CLDHs.

Table

Table List:

Table 1 Kinetic models for the adsorption of Ni and P on CLDHs at 35 and 45 ℃.

Table 2 Langmuir and Freundlich isotherm parameters for adsorption of Ni and P on CLDHs.

Table 3 Comparative studies on the uptake capacities of calcined Mg-Al hydroxides with other reported adsorbents for Ni and P.

Table 4 Thermodynamic parameters for the adsorption of Ni and P on CLDHs as a function of temperature.

Tables:

Table 1

Kinetic models for the adsorption of Ni and P on CLDHs at 35 and 45 °C.

			Pseudo-first-order			Pseudo-second-order			Particle diffusion	
	T (°C)	$q_{e,exp}$ (mg/g)	$q_{e,cal}$ (mg/g)	$K_1(\times10^{-2})$ (/min)	R^2	$q_{e,cal}$ (mg/g)	$K_2(\times10^{-4})$ (g/(mg·min))	R^2	K_i (mg/g $min^{0.5}$)	R^2
Ni	35	17.33	14.77	1.453	0.9760	19.36	13.87	0.9968	0.9716	0.9135
	45	21.46	13.89	1.350	0.9195	22.84	19.68	0.9990	1.168	0.8318
P	35	146.4	115.9	1.138	0.9595	167.2	1.283	0.9983	8.632	0.9173
	45	188.0	133.0	1.357	0.9360	206.2	1.625	0.9988	10.83	0.8606

Table 2

Langmuir and Freundlich isotherm parameters for adsorption of Ni and P on CLDHs.

		Langmuir adsorption model			Freundlich adsorption model		
	T (°C)	Q_{ma} (mg/g)	$K_L(\times10^{-3})$ (L/mg)	R^2	K_F (mg/g)·(L/mg)^n	n	R^2
Ni	25	17.33	854.7	0.9994	12.35	10.22	0.9482
	35	19.15	813.6	0.9995	13.22	9.362	0.9326
	45	21.35	768.6	0.9989	14.36	8.536	0.9695
	55	22.87	761.5	0.9985	14.95	7.753	0.9454
P	25	520.8	3.673	0.9639	9.634	1.742	0.9972
	35	684.9	3.026	0.9549	8.363	1.584	0.9987
	45	1063	2.168	0.8469	7.209	1.422	0.9940
	55	2273	1.406	0.6718	6.380	1.228	0.9935

Table 3

Comparative studies on the uptake capacities of calcined Mg-Al hydroxides with other reported adsorbents for Ni and P.

Adsorbates	Adsorbents	T(°C)	q_m (mg /g)	References
Ni	Calcined Bofe bentonite clay	20	1.910	[29]
	Row doum seed coats	Room temperature	3.240	[30]
	Multiwalled carbon nanotubes	25	6.090	[31]
	Immobilized sericite beads	Room temperature	10.74	[32]
	Hydroxides	—	4.110- 42.84	[16]
	Calcined Mg-Al hydroxides	50	361.1	[33]
	Calcined Mg-Al hydroxides	55	22.87	Present study
P	Nano-bimetal ferrites	45	13.50	[6]
	Activated aluminum oxide	25 ± 1	20.88	[34]
	Bephos™	25 ± 1	26.50	[35]
	Zn-Al hydroxides	30	76.10	[36]
	Calcined Zn-Al hydroxides	30	232.0	[36]
	Calcined Mg-Al hydroxides	25	147.4	[37]
	Calcined Mg-Al hydroxides	55	761.5	Present study

Table 4

Thermodynamic parameters of Ni or P adsorption by CLDHs as a function of temperature.

	ΔG°（kJ/mol)				ΔH°	ΔS°
	298 K	308K	318K	328K	（kJ/mol)	（kJ/mol)
Ni	-6.675	-7.032	-7.397	-7.792	4.394	0.03712
P	-0.04041	-0.2069	-0.4053	-0.5920	5.481	0.01851